HERES, a lncRNA that regulates canonical and noncanonical Wnt signaling pathways via interaction with EZH2

Bo-Hyun You[a,1], Jung-Ho Yoon[b,1], Hoin Kang[c], Eun Kyung Lee[c], Sang Kil Lee[b,d,2], and Jin-Wu Nam[a,e,2]

[a]Department of Life Science, College of Natural Sciences, Hanyang University, 04763 Seoul, Republic of Korea; [b]Division of Gastroenterology, Department of Internal Medicine, Yonsei Institute of Gastroenterology, Yonsei University College of Medicine, 03722 Seoul, Republic of Korea; [c]Department of Biochemistry, College of Medicine, The Catholic University of Korea, 06591 Seoul, Republic of Korea; [d]Brain Korea 21 PLUS Project for Medical Science, Yonsei University, 03722 Seoul, Republic of Korea; and [e]Research Institute for Convergence of Basic Sciences, Hanyang University, 04763 Seoul, Republic of Korea

Edited by Dennis A. Carson, University of California San Diego, La Jolla, CA, and approved October 17, 2019 (received for review July 18, 2019)

Wnt signaling through both canonical and noncanonical pathways plays a core role in development. Dysregulation of these pathways often causes cancer development and progression. Although the pathways independently contribute to the core processes, a regulatory molecule that commonly activates both of them has not yet been reported. Here, we describe a long noncoding RNA (lncRNA), HERES, that epigenetically regulates both canonical and noncanonical Wnt signaling pathways in esophageal squamous cell carcinoma (ESCC). For this study, we performed RNA-seq analysis on Korean ESCC patients and validated these results on a larger ESCC cohort to identify lncRNAs commonly dysregulated in ESCCs. Six of the dysregulated lncRNAs were significantly associated with the clinical outcomes of ESCC patients and defined 4 ESCC subclasses with different prognoses. HERES reduction repressed cell proliferation, migration, invasion, and colony formation in ESCC cell lines and tumor growth in xenograft models. HERES appears to be a transacting factor that regulates *CACNA2D3*, *SFRP2*, and *CXXC4* simultaneously to activate Wnt signaling pathways through an interaction with EZH2 via its G-quadruple structure-like motif. Our results suggest that HERES holds substantial potential as a therapeutic target for ESCC and probably other cancers caused by defects in Wnt signaling pathways.

epigenetic regulation | long noncoding RNA | Wnt signaling pathway | esophageal squamous cell carcinoma

The Wnt signaling pathway is a well-known, evolutionarily conserved pathway that plays important roles in embryonic development; it has also been widely implicated in numerous tumor malignancies (1–4). Wnt signaling can activate both β-catenin–dependent (canonical) and -independent (noncanonical) signal transduction cascades (3, 4). Canonical Wnt signaling results in translocation of the transcriptional activator β-catenin into the nucleus during embryonic development and cell differentiation (5). Constitutive activation of this pathway by various causes leads to developmental diseases and carcinogenesis (6). In contrast, noncanonical Wnt pathways are known to be transduced by Wnt polarity, Wnt-Ca^{2+}, and Wnt-atypical protein kinase signaling, independent of β-catenin transcriptional activity (7). These pathways have also been reported to be independently involved in cancer development as well as embryonic development. In particular, abnormal intracellular levels of the second messenger Ca^{2+} promote the Wnt signaling pathway, which in turn promotes the development and progression of many types of cancers (8).

Controlling Wnt signaling may be a useful strategy for curing cancers caused by aberrations in such signaling. The inhibition of either aberrant canonical or noncanonical Wnt signaling, however, has been shown to decrease progression in only a subset of cancers in a context-dependent manner (9). Because aberrations in Wnt signaling pathways result from various causes, such as mutations in different Wnt signaling-related genes, ligand overexpression, and dysregulation of regulators, targeting only the canonical Wnt signaling pathway might not be a universal therapeutic approach for cancers. Thus, the simultaneous inhibition of aberrant canonical and noncanonical Wnt signaling pathways could also benefit cancer therapy.

Esophageal squamous cell carcinoma (ESCC), a major histological type of primary esophageal cancer in east Asia and other developing countries, is associated with a very poor survival rate that is only 5–15% at 5 y (10, 11), mainly due to delayed diagnosis, a high rate of metastasis, and a lack of effective treatment strategies (10–12). Moreover, the benefits of curative surgery for advanced stages of ESCC are still unclear (11, 13), and although cisplatin-based chemotherapy is commonly used, the effects are inconsistent among individuals (12, 14). Despite ongoing trials with combination therapy, efforts to identify appropriate targets

Significance

Aberrant lncRNA expression is responsible for cancer progression and metastasis, positioning lncRNAs not only as biomarkers but also as promising therapeutic targets for curing cancer. A number of lncRNAs have been reported in ESCC but their mechanistic roles largely remain unknown. Wnt signaling pathways are often dysregulated in ESCC; however, the role of lncRNAs in such dysregulation was also undetermined. We found 6 lncRNAs that are significantly dysregulated and correlated with outcomes in ESCC patients. The most upregulated lncRNA, HERES, promotes cancer progression and epigenetically regulates canonical and noncanonical Wnt signaling pathways simultaneously through interaction with EZH2. These results show that HERES represents an early diagnostic and therapeutic target for squamous-cell-type cancers caused by defects in Wnt signaling pathways.

Author contributions: S.K.L. and J.-W.N. designed research; B.-H.Y., J.-H.Y., H.K., and E.K.L. performed research; B.-H.Y. analyzed data; and B.-H.Y., J.-H.Y., S.K.L., and J.-W.N. wrote the paper.

The authors declare no competing interest.

This article is a PNAS Direct Submission.

Data deposition: Raw RNA-seq data and expression tables from ESCC patients have been deposited in the National Center for Biotechnology Information (NCBI) Gene Expression Omnibus (GEO) database, https://www.ncbi.nlm.nih.gov/geo/ (accession no. GSE130078). LncRNA annotation constructed in this study can be downloaded from our website (http://big.hanyang.ac.kr/CASOL/catalog.html).

[1]B.-H.Y. and J.-H.Y. contributed equally to this work.

[2]To whom correspondence may be addressed. Email: sklee@yuhs.ac or jwnam@hanyang.ac.kr.

This article contains supporting information online at https://www.pnas.org/lookup/suppl/doi:10.1073/pnas.1912126116/-/DCSupplemental.

First published November 15, 2019.

to improve the therapy for ESCC have been largely unsuccessful (15, 16).

Long noncoding RNAs (lncRNAs), defined as transcripts longer than 200 nt that do not code for functional proteins (17, 18), have been proposed as regulators of critical biological processes and cancer-related mechanisms (19–21). Because lncRNAs can modulate multiple targets at the transcriptional and post-transcriptional levels, lncRNAs tend to play functional roles in more than 1 biological pathway. Moreover, mounting evidence indicates that aberrant lncRNA expression, by modulating cancer-related pathways, can be responsible for cancer progression (22, 23). To date, hundreds of lncRNAs have been reported to be dysregulated in cancers and dozens of them have been known to be associated with cancer progression. With respect to ESCC development, the function of a few lncRNAs, including LUCAT1 and CASC9, have been investigated via a candidate-gene approach (24, 25). Recently, a Chinese group performed high-throughput RNA sequencing (RNA-seq) on tissue from 15 paired ESCC patients and normal individuals and identified lncRNAs dysregulated in ESCCs (26). Furthermore, they described a lncRNA that affects cell proliferation and invasion in ESCC cell lines but did not determine a mechanism of action. Thus, the identification of ESCC-driving lncRNAs and an investigation of their cancer-driving mechanisms have not been simultaneously carried out.

Through integrative analyses of ESCC-driving lncRNAs, we found 6 lncRNAs associated with cancer progression and relapse. We also determined that a lncRNA, HERES (highly

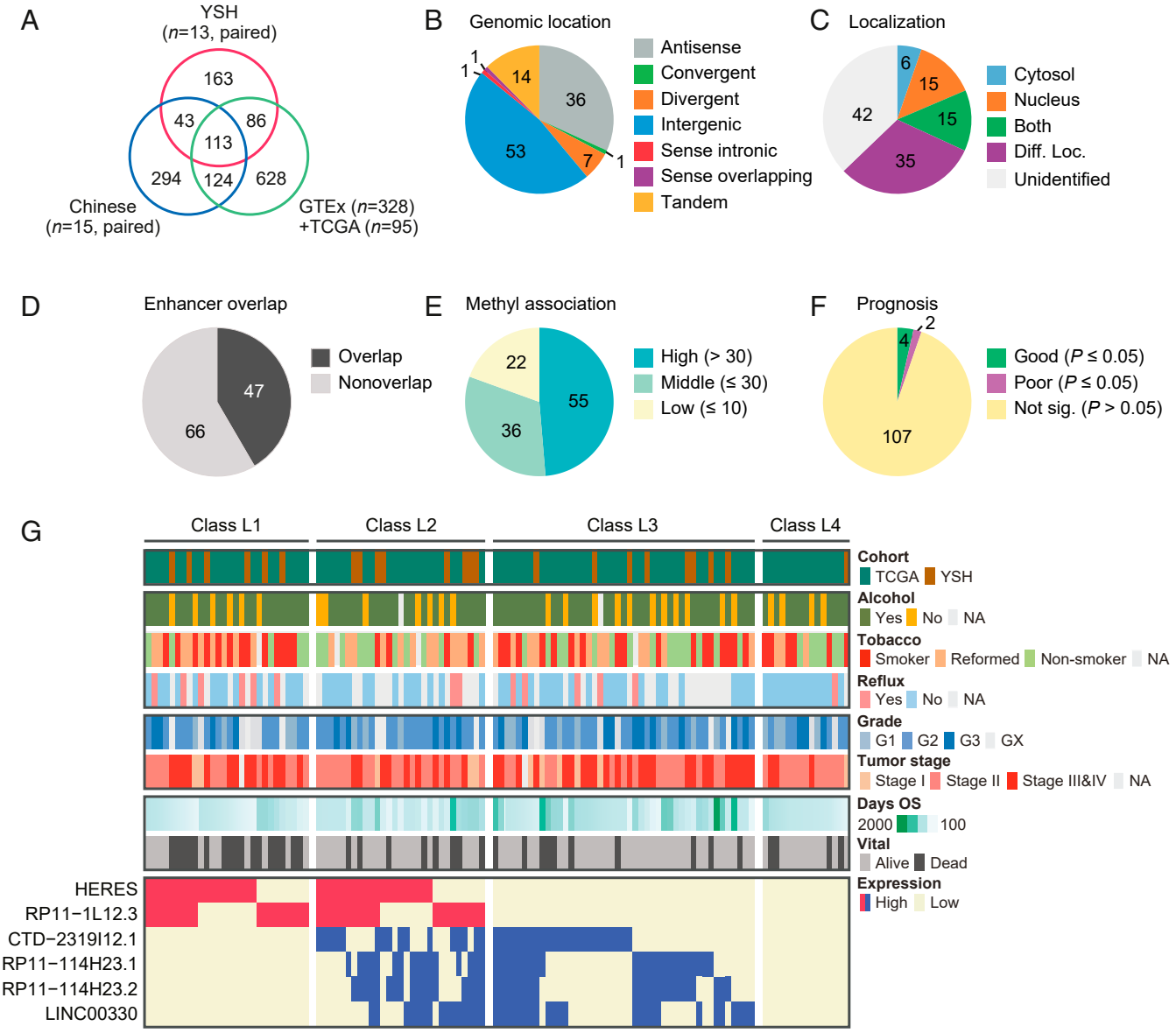

Fig. 1. Characterization of a common set of DE lncRNAs in ESCC. (*A*) Venn diagram of the DE lncRNAs detected in 3 ESCC cohorts (YSH, Chinese, and GTEx+TCGA). The pie charts (*B*–*F*) show the number of DE lncRNAs categorized according to their genomic location (*B*), subcellular localization (*C*), enhancer overlap (*D*), association with DNA methylation (*E*), and prognostic power (*F*). (*G*) The 4 ESCC subclasses based on the 6 prognostic marker lncRNAs in *F*. The top section presents cohort information, clinical history, pathological features, and survival information from the YSH and TCGA ESCC patients. The various categories are represented as different colors, as shown in the legend on the right. OS is overall survival. The expression patterns of the 6 prognosis-related lncRNAs in the RNA-seq datasets are shown with a colored heatmap in the bottom section (red indicates the top 33% highly expressed lncRNAs associated with a HHR; blue indicates the top 33% highly expressed lncRNAs associated with a LHR).

expressed lncRNA in esophageal squamous cell carcinoma), promoted tumor progression by regulating components of the canonical and noncanonical Wnt signaling pathways via interaction with EZH2, a subunit of polycomb repressive complex 2 (PRC2).

Results

High-Confidence Differentially Expressed (DE) lncRNAs in ESCC. To identify a set of lncRNAs dysregulated in ESCC, RNA-seq performed from paired cancerous and noncancerous tissues of 13 ESCC patients in the Yonsei Severance Hospital (YSH) cohort (Dataset S1) and was subjected to transcriptome assembly, and lncRNA annotations using our computational pipeline (27) (*SI Appendix*, Fig. S1). In total, 6,411 lncRNAs from 4,842 annotated loci and 1,924 from 1,657 unannotated loci were identified (Dataset S2). Of the total of 8,335 lncRNAs, 465 (305 up-regulated and 160 down-regulated) were significantly dysregulated in ESCC, exhibiting greater than 2-fold differences in expression, with a false discovery rate (FDR) ≤ 0.01 (Fig. 1*A* and Dataset S3). Then, to identify an ethnically independent set of DE lncRNAs in ESCC, 113 DE lncRNAs commonly dysregulated in all 3 ESCC cohorts (YSH, Genotype-Tissue Expression [GTEx] + The Cancer Genome Atlas [TCGA], and Chinese) were selected (Fig. 1*A*). Of the 113 confidence DE lncRNAs, 20 were newly annotated, 32 were up-regulated, and 81 were down-regulated in ESCC (*SI Appendix*, Fig. S2 *A–C*). A majority of the confidence DE lncRNA genes were either located in intergenic regions or were antisense to other genes (Fig. 1*B*); their genomic and clinical features, such as subcellular localization of the lncRNA (Fig. 1*C*), associations with enhancers (Fig. 1*D*), and DNA methylation (Fig. 1*E*), were systematically examined (Dataset S4 *A–D*). As previously reported, many overlapped with enhancers (Fig. 1*D*) and seemed to be associated with epigenetic markers of other genes (Fig. 1*E*).

Six lncRNAs Define 4 ESCC Subclasses with Different Clinical Outcomes. To find clinically relevant lncRNAs that are associated with survival outcomes of patients, Kaplan–Meier survival analysis for all 113 DE lncRNAs were performed with TCGA ESCC datasets comprising 95 patient samples (Fig. 1*F* and Dataset S4*E*). Six DE lncRNAs were significantly associated with survival rates, 2 (HERES and RP11-1L12.3) of which were associated with a high hazard ratio (HHR; $P \leq 0.05$) and 4 (RP11-114H23.1, RP11-114H23.2, CTD-2319I12.1, and LINC00330) of which were associated with a low hazard ratio (LHR; $P \leq 0.05$). To delineate how the expression of the 6 lncRNAs stratifies ESCC patients, we clustered samples from the TCGA and YSH cohorts including additional 10 RNA-seq samples where the clinical values were available based on the binary expression patterns (high and low) of the 6 lncRNAs, revealing 4 distinct classes of patients: class L1~L4 (Fig. 1*G* and Dataset S5). Noticeably, class L1, in which only the HHR markers are highly expressed, showed a worse survival rate than class L3 ($P < 0.05$) and the other classes ($P = 0.01$; Fisher's exact test). Class L3 tended to display a greater overall survival rate than other classes ($P < 0.05$; Fisher's exact test). Importantly, class L1 appeared to be significantly associated with smoking ($P < 0.05$; Fisher's exact test), compared to other classes. Taken together, these results indicate that the 6 lncRNAs represent prognostic signature genes that can stratify ESCC patients based on clinical outcomes.

***HERES* Encodes Alternative Splicing Isoforms, Up-Regulated in ESCCs.** Since HERES, 1 of the HHR markers, was greatly up-regulated in ESCCs compared to paired adjacent noncancerous samples (*SI Appendix*, Fig. S3) and most strongly associated with poor vital status (Fig. 1*G*), we investigated whether HERES might be an ESCC-driving lncRNA. The lncRNA gene encodes 2 isoforms with the same transcription start sites (TSSs) (28) and cleavage and polyadenylation sites (CPSs) (29) (Fig. 2*A*). Isoform #1, HERES.1, is 2,160 nt and contains 2 exons, whereas isoform #2,

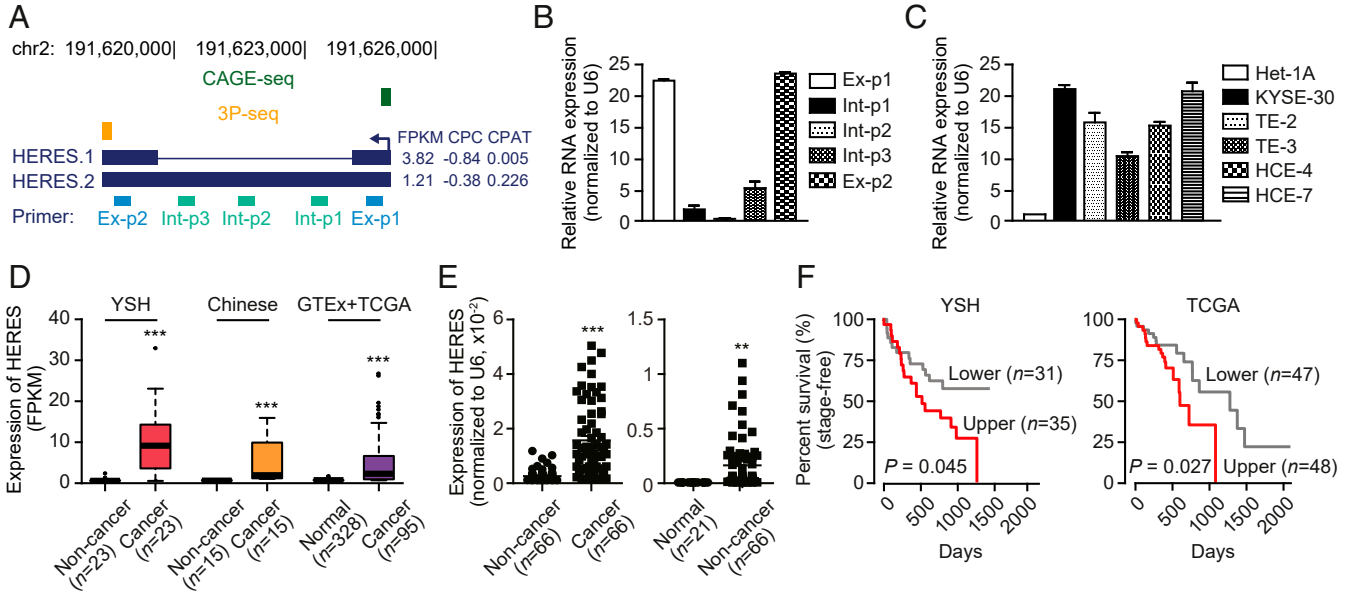

Fig. 2. *HERES* is a highly expressed lncRNA in ESCC. (*A*) The *HERES* genomic locus with CAGE-seq and 3P-seq signals. qRT-PCR primer sets were designed to recognize exonic (2) and intronic regions (3). The coding potentials calculated by CPC and CPAT are indicated on the right. (*B*) qRT-PCR results using the 5 primer sets in KYSE-30 cells. (*C*) The *HERES* expression level was measured in 5 ESCC cell lines and a normal esophageal cell line (Het-1A). (*B* and *C*) Error bars represent the mean ± SD from 3 independent experiments. (*D*) The box plots show the *HERES* expression levels in normal, noncancerous, and cancerous tissues from the YSH cohort (paired), the Chinese cohort (paired), and the TCGA cohort. (*E*) *HERES* expression levels measured by qRT-PCR in additional frozen tissue samples including YSH ESCC ($n = 66$) and adjacent samples (noncancer; $n = 66$) (*Left*) and in normal mucosa tissues ($n = 21$) from reflux symptom patients (*Right*). (*F*) Survival analyses of YSH and TCGA patients from whom the ESCC samples were obtained based on the *HERES* expression level. $^{**}P \leq 0.01$, $^{***}P \leq 0.001$.

HERES.2, is an intron-retained, single-exonic transcript that is 6675 nt. Both isoforms were confirmed to lack coding potential (Fig. 2*A*). Analysis of ESCC RNA-seq datasets (*SI Appendix*, Fig. S4*A*) and qRT-PCR in an ESCC cell line (KYSE-30) (Fig. 2 *A* and *B*) showed that HERES.1 is the major isoform. Only a short region in *HERES* exon 1 displays sequence conservation with a region in the mouse genome; the intergenic *HERES* locus between the *GLS* and *NAB1* genes on chromosome 2 shows synteny conservation in mouse (*SI Appendix*, Fig. S4*B*).

Elevated *HERES* expression was then validated in other ESCC cell lines. Compared to that in a normal esophageal epithelial cell line (Het-1A), *HERES* expression appeared to be up-regulated greater than 10-fold in all tested ESCC cell lines (Fig. 2*C*), as observed in ESCC samples (Fig. 2*D*). *HERES* was significantly up-regulated not only in ESCC, but also in esophageal adenocarcinoma (ESAD) and other squamous carcinomas (head and neck, and lung squamous cell carcinoma; HNSC and LUSC), but not in lung adenocarcinoma (LUAD) (*SI Appendix*, Fig. S4*C*). These expression changes were further confirmed in 66 ESCC samples from the YSH cohort using qRT-PCR, which revealed an elevated level of *HERES* in cancers compared to adjacent noncancerous samples (Fig. 2 *E*, *Left*). *HERES* expression in the adjacent noncancerous samples was higher than that in normal mucosa from the normal population (Fig. 2 *E*, *Right*). As observed in the YSH cohort (Fig. 2 *F*, *Left* and Dataset S6), *HERES* levels were significantly correlated with stage-free survival rates in the TCGA ESCC cohort (Fig. 2 *F*, *Right*), and multivariate analysis with clinical information revealed that the *HERES* level was strongly associated with tumor grade ($P = 0.004$; Fisher's exact test) but not with other clinicopathological factors (*SI Appendix*, Fig. S4*D*).

HERES Promotes Cell Proliferation, Migration, Invasion, and Colony Formation. To investigate whether HERES is involved in cancer development and progression, the effects of HERES knockdown on cell proliferation, migration, invasion, and colony formation were explored with siControl- and siHERES-treated cells. Introduction

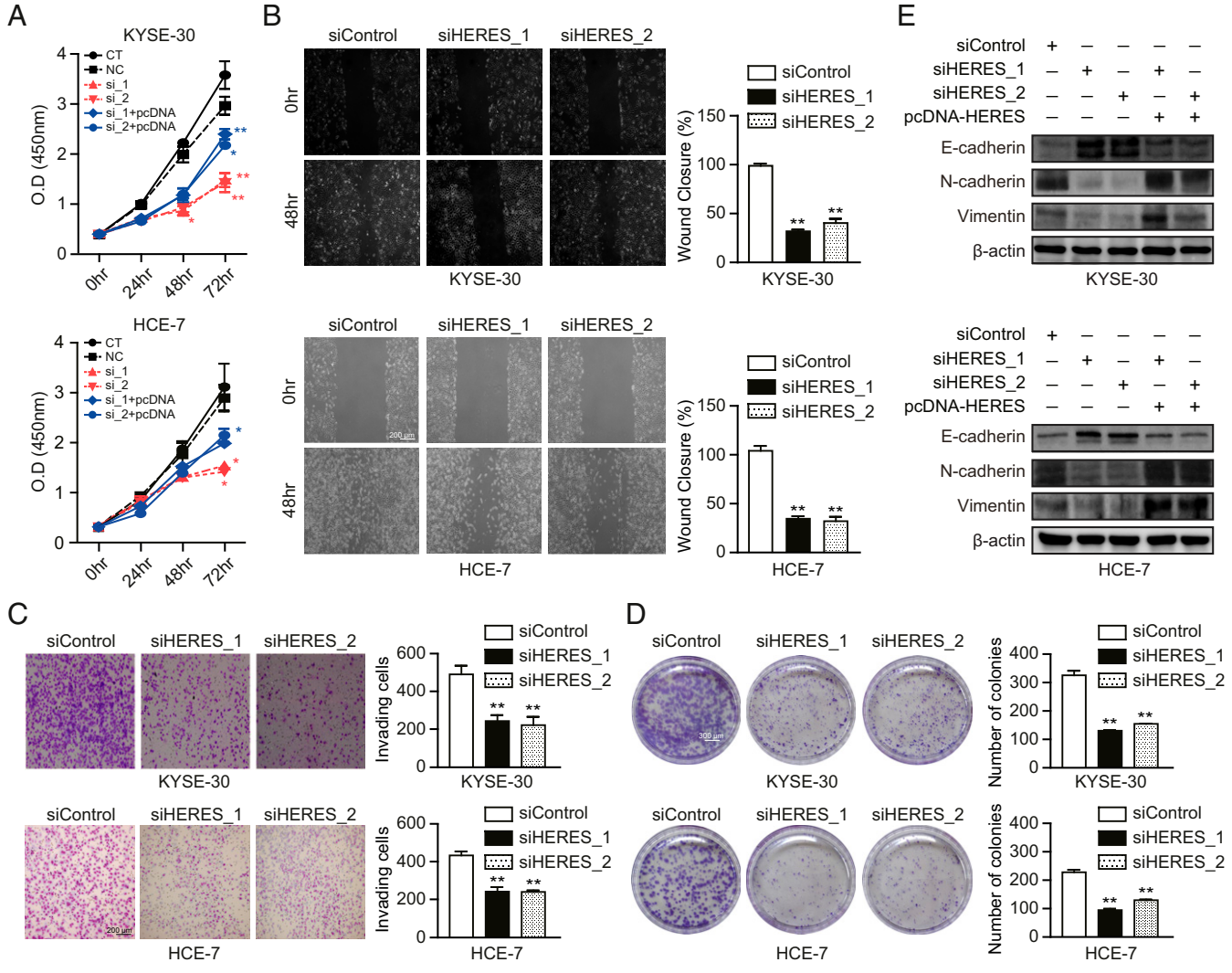

Fig. 3. HERES modulates cell proliferation, migration, invasion, and colony formation. (*A*) Cell viability was measured using an MTS assay in KYSE-30 and HCE-7 cells transfected with siControl (NC), siHERES (si_1 and si_2), or siHERES followed by pcDNA-HERES (si_1+pcDNA, si_2+pcDNA). Growth curves were compared between siHERES- and siControl-transfected cells, and between pcDNA-HERES+siHERES- and siHERES-transfected cells. Wound healing assays (*B*), invasion assays (*C*), and colony formation assays (*D*) were performed in KYSE-30 and HCE-7 cells after HERES knockdown (all assay images at 4× magnification). The bar graphs represent the frequency of wound closure (*B*) and the number of invading cells (*C*) and colonies formed (*D*). Data represent the mean ± SD from 3 independent experiments (*A*–*D*). (*E*) Expression of EMT markers in KYSE-30 and HCE-7 cells transfected with siControl or the indicated combinations of siHERES and pcDNA-HERES as determined by immunoblot. $*P \leq 0.05$, $**P \leq 0.01$.

of an siRNA targeting HERES (siHERES_1 or siHERES_2) to KYSE-30 and HCE-7 cells significantly reduced *HERES* expression (*SI Appendix*, Fig. S5). The proliferation indices (optical density [O.D.] values) were significantly reduced in both siHERES_1 and siHERES_2-treated cells compared to siControl-treated cells (Fig. 3*A*), and the introduction of a *HERES* pcDNA expression construct partly rescued the proliferation activity (Fig. 3*A*), indicating that HERES can regulate cell proliferation. Migration and invasion assays showed that both cell migration and invasion were greatly reduced in siHERES-treated cells compared to siControl-treated cells (Fig. 3 *B* and *C*). In addition, HERES knockdown also reduced colony formation measured at 14 d after siRNA transfection (Fig. 3*D*). A role for HERES in malignant ESCC progression was confirmed by the reduction of N-cadherin and vimentin levels in siHERES-treated cells and by the rescue of these levels by the introduction of the *HERES* pcDNA construct to the cells (Fig. 3*E* and *SI Appendix*, Fig. S6). These results suggest that HERES can promote cancer progression and metastasis.

HERES Affects Wnt Signaling Pathway-Related Genes. To study the means by which HERES promotes cancer development and progression, the changes in expression of ∼730 cancer-related pathway genes were analyzed in siHERES-treated and siControl-treated KYSE-30 cells using the NanoString nCounter PanCancer Pathways Panel (Fig. 4*A* and Dataset S7). Seventy-seven cancer-related genes (34 for up-regulation and 43 for down-regulation) were dysregulated greater than 2-fold in siHERES-treated cells compared to siControl cells (Fig. 4*A*); the expression changes of the 2 most up-regulated genes (*CACNA2D3* and *SFRP2*) and the 2 most down-regulated genes (*BMP7* and *GRIN1*) in this group were confirmed by qRT-PCR (*SI Appendix*, Fig. S7 *A–D*). Noticeably, among the genes dysregulated by HERES reduction, 14 belong to the Wnt signaling pathway, and half of the 10 most up-regulated genes (*CACNA2D3*, *SFRP2*, *CACNA1E*, *CXXC4*, and *SFRP4*) are involved in the Wnt signaling pathway (Dataset S7). *CACNA2D3*, which encodes a subunit of the calcium channel protein complex, was previously shown to be induced in ESCC (30) and other cancers (31, 32) via epigenetic mechanisms, and its down-regulation led to inactivation of Wnt/Ca^{2+} signaling pathway (32). *SFRP2* encodes a member of the SFRP family that modulates the Wnt signaling pathway; *SFRP2* hypermethylation is known to enhance cell invasiveness in both cancers and noncancerous diseases (33, 34). The enrichment of canonical and noncanonical Wnt signaling pathway-related genes among the genes that respond to HERES depletion, together with results from previous studies, suggest that HERES may regulate cancer development via control of Wnt signaling pathways.

HERES Regulates Wnt Signaling Pathways at the Epigenetic Level. As HERES appeared to be enriched in the nucleus rather than the cytoplasm (Fig. 4*B* and *SI Appendix*, Fig. S2*C*) and nucleus-localized lncRNAs are often reported to be epigenetic regulators, a potential epigenetic role for HERES was investigated by analyzing publicly available array-based DNA methylation and RNA-seq data from TCGA ESCC samples. Based on their *HERES* expression level, the ESCC samples were first divided into 2 subgroups, HERES-high and HERES-low, and the changes in expression and DNA methylation of the protein-coding genes were then compared between the subgroups (Fig. 4*C* and Dataset S8). Of the genes, *CACNA2D3* and *LDOC1* (Fig. 4*D* and *SI Appendix*, Fig. S7*E*) were down-regulated and hypermethylated in the HERES-high group, whereas *EPSTI1*, *SLC15A3*, and *BST2* were up-regulated and hypomethylated in the HERES-high subgroup. The expression and DNA methylation changes were confirmed in HERES-depleted KYSE-30 cells by qRT-PCR and methylation-specific (MS) PCR. Only 2 down-regulated genes (*CACNA2D3* and *LDOC1*) were confirmed to have both expression and DNA methylation changes (Fig. 4*E* and *SI Appendix*, Fig. S7 *F–L*). On the other hand, although *SFRP2* and *CXXC4* did not display DNA methylation changes in the analysis of the TCGA ESCC samples, the expression and DNA methylation signals of the Wnt signaling-related genes were changed similarly to those of *CACNA2D3* and *LDOC1* in the siHERES-treated cells compared to the siControl-treated cells (*SI Appendix*, Fig. S7*B* and S8 *A–C*).

Because DNA methylation is often associated with histone modifications (35, 36), global changes in histone modification markers in response to HERES knockdown were examined, revealing a marked decrease in H3K27me3 levels (Fig. 4*F*). We then investigated where the H3K27me3 signal was depleted in the genomic regions of 3 Wnt signaling pathway genes in siHERES-treated cells using chromatin immunoprecipitation (ChIP)-qPCR analysis. Significantly reduced H3K27me3 signals were observed at specific sites in the genes (recognized by primer 5 for *CACNA2D3*, primers 3, 4, and 5 for *SFRP2*, and primers 9 and 10 for *CXXC4*) in siHERES-depleted cells (Fig. 4*G* and *SI Appendix*, Fig. S8 *D* and *E*).

Previous studies reported that CACNA2D3 down-regulation inhibited the noncanonical Wnt/Ca^{2+} signaling pathway by decreasing the intracellular calcium level and NLK expression (32) and that SFRP2 and CXXC4 play roles as negative regulators of the canonical Wnt signaling pathway (34, 37). We thus examined changes in the expression of 2 Wnt signaling-related factors, NLK and β-catenin, in siHERES-treated cells (Fig. 4*H* and *SI Appendix*, Fig. S9). As expected, HERES reduction increased the NLK level and decreased β-catenin in KYSE-30 and HCE-7 cells. In addition, changes in the expression of Wnt downstream targets were also confirmed (Fig. 4*H* and *SI Appendix*, Fig. S9). In contrast, introducing the pcDNA-HERES construct to cells reverted the expression levels of NLK, β-catenin, and Wnt downstream targets (Fig. 4*H* and *SI Appendix*, Fig. S9). Taken together, these results suggest that HERES down-regulation in cancers perturbs and promotes canonical and noncanonical Wnt signaling pathways via epigenetic regulation, resulting in the inhibition of cancer progression.

Inhibition of HERES Arrests the Cell Cycle at the G1/S Checkpoint and Induces Apoptosis. Because 2 of the downstream targets of HERES, *CCND1* and *CACNA2D3*, are known to regulate the cell cycle and apoptosis (30, 32), the effect of the loss of HERES on the cell cycle and apoptotic processes was examined. Cell counting showed that siHERES-treated cells were arrested at G0/G1 (Fig. 5*A*). Flow cytometry showed that siHERES-treated cell populations exhibited significantly increased levels of apoptosis compared to siControl-treated cells (Fig. 5*B*). An induction of apoptotic factors, such as cleavage of poly (ADP ribose) polymerase (PARP), cleaved caspase-9, and Bax, and a reduction of the anti-apoptotic factor, Bcl-2, were confirmed in siHERES-treated cells. However, the rescue of HERES expression reverted the expression of these factors to levels in control cells (Fig. 5*C*).

HERES Interacts with EZH2 to Regulate *CACNA2D3*. We then asked how HERES regulates the expression of target genes at the epigenetic level. To address this question, binding sites for possible epigenetic modulators that can drive the histone methylation of target genes were first examined using publicly available ChIP-seq datasets from the ENCODE project. We found that all 3 HERES target genes contained enhancer of EZH2 binding sites in their promoter regions (*SI Appendix*, Fig. S10). Because EZH2, a subunit of the PRC2, has a well-known role in histone methylation to generate H3K27me3 and is known to interact with nuclear lncRNAs (38), we suspected that EZH2 would be a binding partner of HERES. To examine the molecular relationship between HERES and EZH2, EZH2 RNA and protein levels were quantified in siControl- and siHERES-treated KYSE-30 cells, showing that HERES reduction decreased the EZH2 protein level but not

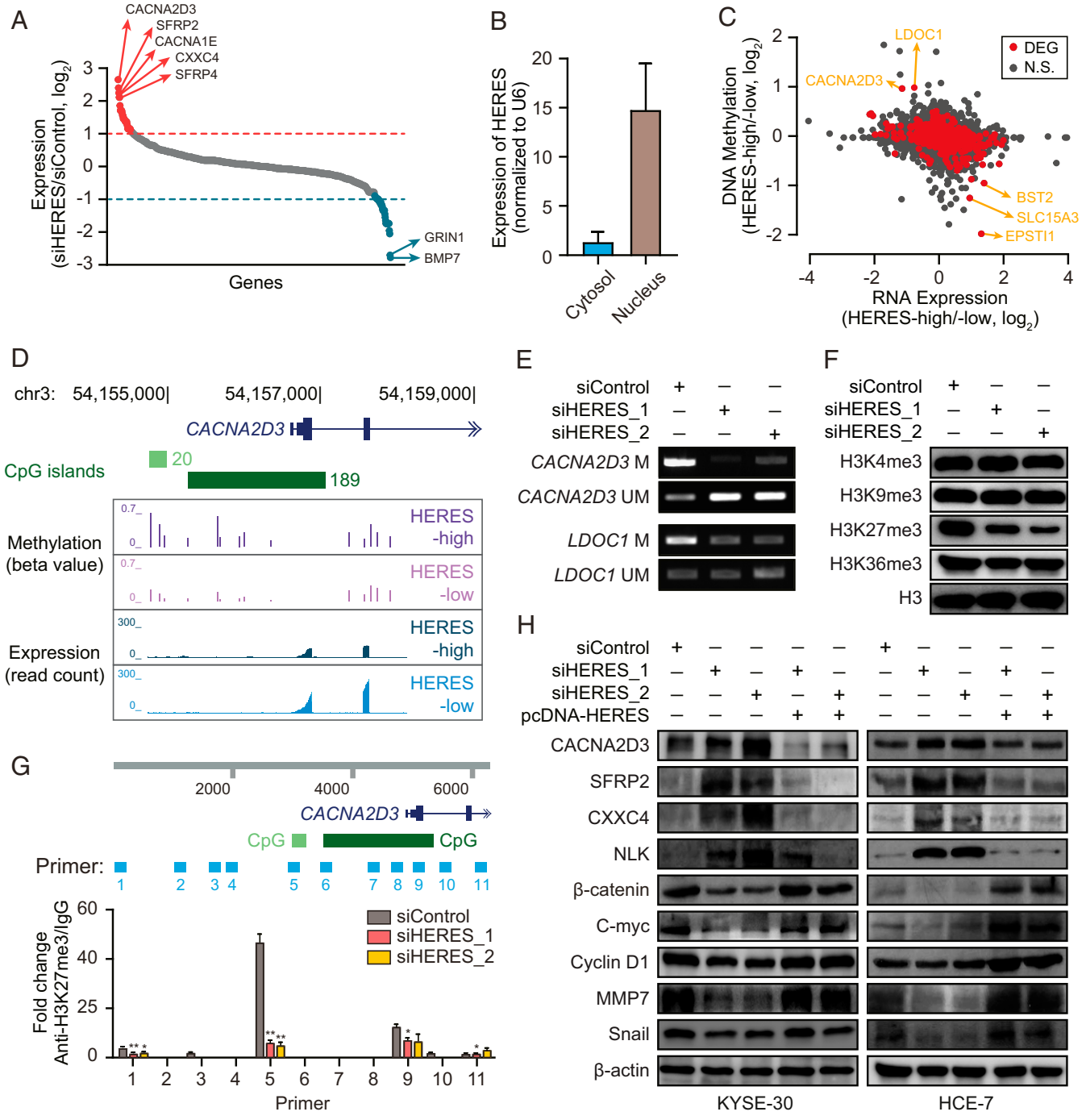

Fig. 4. HERES epigenetically regulates genes involved in canonical and noncanonical Wnt signaling pathways. (*A*) Changes in the expression of cancer-related genes in response to siHERES treatment compared to siControl are shown. The colored circles indicate genes that are up-regulated (red) or down-regulated (blue) under HERES-depleted conditions. Changes in the expression of the highlighted genes were experimentally confirmed by qRT-PCR. (*B*) HERES expression in the nuclear and cytoplasmic fractions of KYSE-30 cells as determined by qRT-PCR. (*C*) Log-scaled fold-changes of expression (*x* axis) and DNA methylation (*y* axis) of each gene in the HERES-high versus HERES-low sample groups from the TCGA dataset. The red dots indicate DE genes in ESCC. The highlighted genes are those for which there is anti-correlation between expression and DNA methylation. DEG: DE gene. N.S.: not significant. (*D*) The *CACNA2D3* genomic locus with CpG island tracks, DNA methylation (beta value), and RNA expression (read count) in the HERES-high and HERES-low groups. (*E*) *CACNA2D3* and *LDOC1* DNA methylation patterns (methylation [M] and unmethylation [UM]) were measured by MS-PCR in KYSE-30 cells transfected with siControl or siHERES. (*F*) Immunoblots of histone modification markers in siControl- or siHERES-transfected KYSE-30 cells. (*G*) ChIP-qPCR analysis of the H3K27me3 level of *CACNA2D3* in siControl- or siHERES-transfected KYSE-30 cells. Data represent the mean ± SD from 3 independent experiments. (*H*) Immunoblots of the products of the 3 HERES target genes (CACNA2D3, SFRP2, and CXXC4), components (β-catenin and NLK) of the Wnt/β-catenin and Wnt/Ca^{2+} signaling pathways, and downstream proteins associated with cell proliferation (CMYC and CCND1), invasion (MMP7), and EMT (SNAIL).

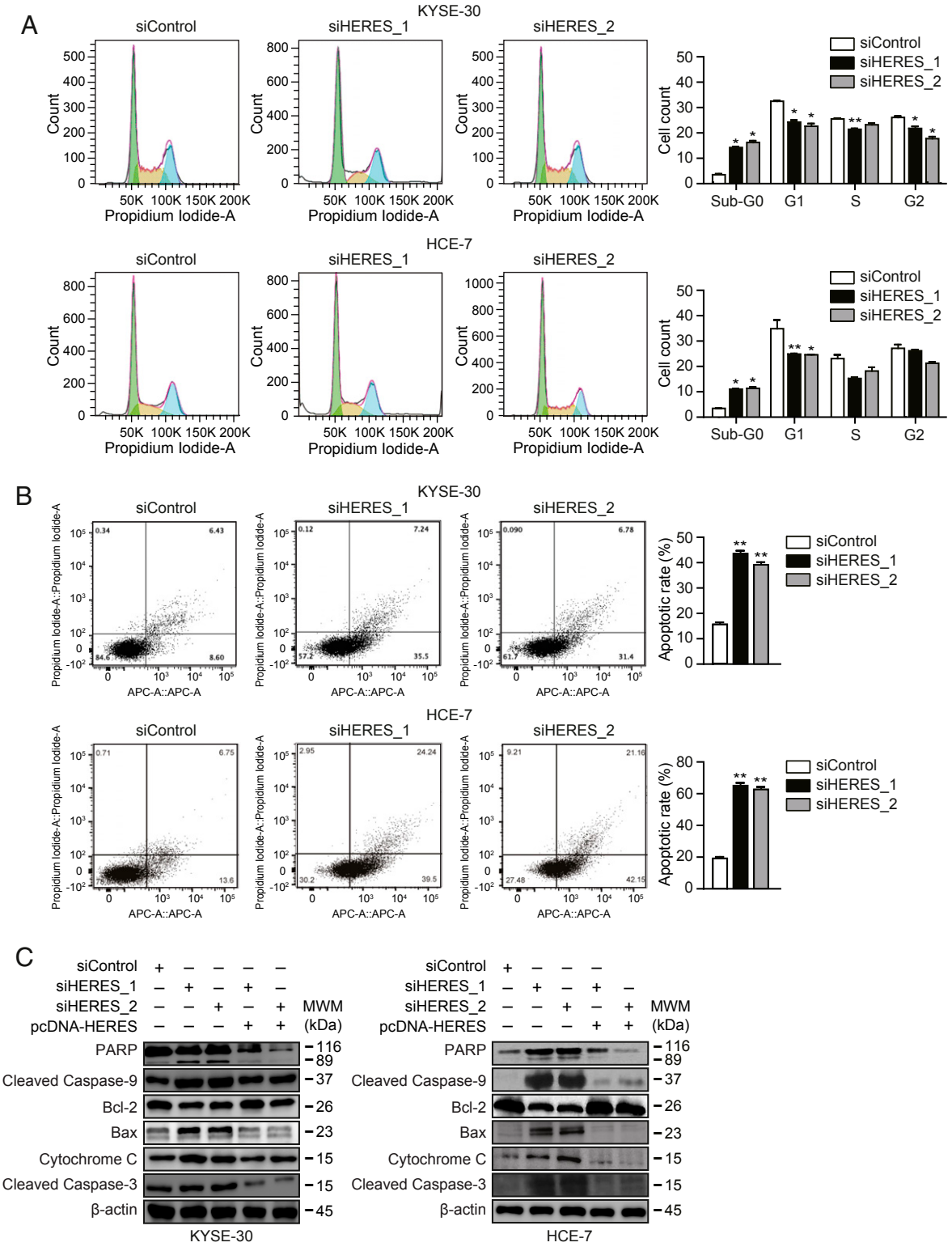

Fig. 5. The effect of HERES on the cell cycle and apoptosis. Cell cycle (*A*) and apoptosis (*B*) assays were performed on siRNA-transfected KYSE-30 and HCE-7 cells. (*A*) Cell cycle analysis of siRNA-transfected KYSE-30 and HCE-7 cells by flow cytometry. The bar graph shows the percentage of cells in sub-G0, G1, S, and G2 phases in siRNA-transfected KYSE-30 and HCE-7 cell populations. (*B*) Apoptosis was measured by flow cytometry using PI/Annexin V staining. The bar graph represents the percentage of apoptotic cells in each population. Data represent the mean ± SD from 3 independent experiments. (*C*) Apoptosis markers were assessed by immunoblot in KYSE-30 and HCE-7 cells transfected with siControl or siHERES and/or pcDNA-HERES. $*P \leq 0.05$, $**P \leq 0.01$.

the RNA level (Fig. 6*A* and *SI Appendix*, Fig. S11*A*). Subsequently, RNA immunoprecipitation (RIP) (Fig. 6*B*) and EZH2 IP (Fig. 6*C*) assays showed the interaction of HERES and *CACNA2D3* with EZH2. To validate a direct interaction between HERES and PRC2-EZH2, we then searched for PRC2-EZH2 binding motifs in the HERES sequence. Because the PRC2 complex including

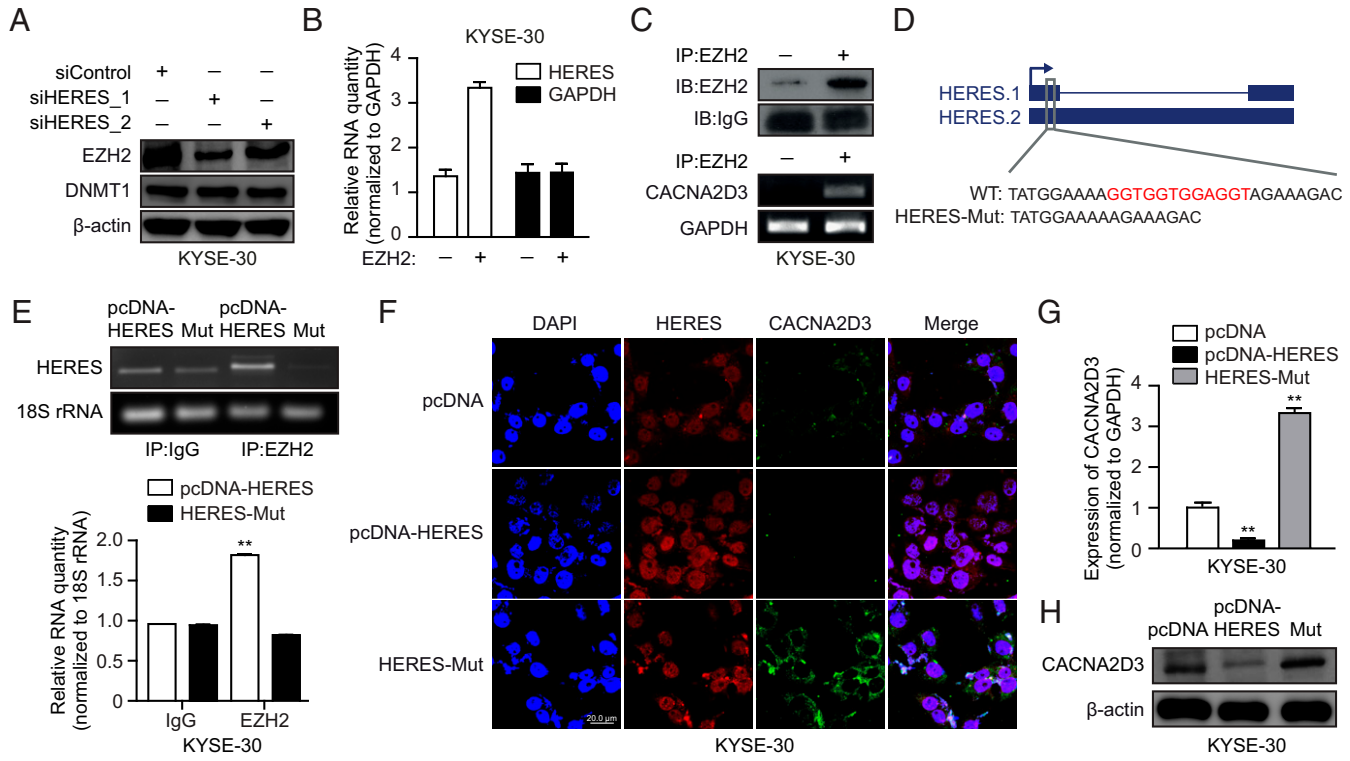

Fig. 6. HERES regulates CACNA2D3 via interaction with EZH2. (*A*) Immunoblots of EZH2 and DNMT1 in KYSE-30 cells transfected with either siControl or siHERES. (*B*) RIP assays were performed with anti-EZH2 in KYSE-30 cell lysates. The quantity of HERES in the cell lysates (input) and the immunoprecipitates was measured by qRT-PCR. (*C*) IP assays were performed with anti-EZH2 in KYSE-30 cell lysates. The quantity of CACNA2D3 in the cell lysates (input) and the immunoprecipitates was measured by immunoblot. (*D*) Representation of the WT and mutated (HERES-Mut) HERES sequences used for IP with anti-EZH2. HERES-Mut contains a deletion of the G-rich sequence (index 1) presented in *SI Appendix*, Fig. S11*B*. (*E*) RIP assays were performed with anti-EZH2 in lysates of KYSE-30 cells transfected with either pcDNA-HERES or HERES-Mut (*Upper*). The bar graph shows the relative amount of HERES after anti-EZH2 IP using lysates of cells transfected with either pcDNA-HERES or HERES-Mut (*Lower*). (*F*) RNA FISH (40× magnification) to visualize HERES (red) and FITC staining of CACNA2D3 (green) in KYSE-30 cells transfected with pcDNA (*Upper*), pcDNA-HERES (*Middle*), or HERES-Mut (*Lower*). (Scale bar, 20 μm.) Nuclei were stained with 4′,6-diamidino-2-phenylindole (DAPI) (blue). CACNA2D3 RNA (*G*) and protein (*H*) levels were measured in KYSE-30 cells transfected with pcDNA, pcDNA-HERES, or HERES-Mut by qRT-PCR and immunoblot, respectively. Data represent the mean ± SD from 3 independent experiments (*B*, *E*, and *G*). $^{**}P \leq 0.01$.

EZH2 is known to be recruited by G-rich motifs (39), we scanned for G-rich regions in HERES transcripts, leading to the identification of 6 regions including 2 potential g-quadruple structure motifs (*SI Appendix*, Fig. S11*B*). EZH2-IP and qRT-PCR showed that a single region with 4 GGW repeats (index 1) was significantly enriched in EZH2-IP (*SI Appendix*, Fig. S11*C*). To further investigate if the HERES GGW repeat sequence (index 1) is necessary for an interaction with EZH2, we constructed a plasmid vector that harbors a HERES sequence that lacks the GGW repeat region (HERES-Mut) (Fig. 6*D*). A RIP assay confirmed that EZH2 failed to interact with HERES-Mut in KYSE-30 cells (Fig. 6*E*). RNA fluorescence in situ hybridization (FISH) of HERES and fluorescein isothiocyanate (FITC) staining of CACNA2D3 validated that HERES was principally localized to the nucleus and that the GGW sequence (index 1) is necessary for the interaction with EZH2 to down-regulate CACNA2D3 (Fig. 6*F*). Cells transfected with HERES-Mut exhibited significantly increased CACNA2D3 at both the RNA and protein level, whereas HERES overexpression (pcDNA-HERES) reduced the CACNA2D3 level (Fig. 6 *G* and *H*).

HERES as a Candidate Therapeutic Target. To investigate whether HERES controls tumor growth in vivo, we carried out xenograft assays with siControl- and siHERES-treated cancer cell lines (Fig. 7). Both the volume and weight of tumors derived from HERES-depleted samples were significantly reduced compared to tumors derived from control cells 4 wk after the injection (Fig. 7 *A*–*C*). We further examined changes in the expression of HERES and its target genes, finding that the reduction of HERES was maintained for 4 wk after siHERES injection (*SI Appendix*, Fig. S12), whereas the levels of HERES targets were significantly increased in tumor samples derived from HERES-depleted cells compared to control cells (Fig. 7*D*). We also confirmed that global H3K27me3 and EZH2 levels were decreased in HERES-depleted tumor samples (Fig. 7*D*), suggesting that HERES is a promising candidate therapeutic target that controls tumor growth through the regulation of canonical and noncanonical Wnt signaling pathways in vivo (Fig. 7*E*).

Discussion

A series of computational and experimental analyses showed that HERES transcriptionally controls multiple target genes in the Wnt signaling pathways at the epigenetic level by interacting with the EZH2-PRC2 complex. Because the targets and *HERES* are generally located on different chromosomes, HERES appears to act via EZH2-PRC2 in *trans* rather than in *cis*. Intriguingly, HERES RNA contains some repeat elements including GGW and Alu repeats, which extensively match sequences in the upstream regions of the target genes including *CACNA2D3* (*SI Appendix*, Fig. S13). Particularly, the Alu repeats would provide complementary base-pairing between HERES its target DNA sequences as well as it might be related to the nuclear localization of HERES, as previously reported (40).

Although we reported in this study that a G-rich motif in HERES is important for binding to EZH2, it remains unclear

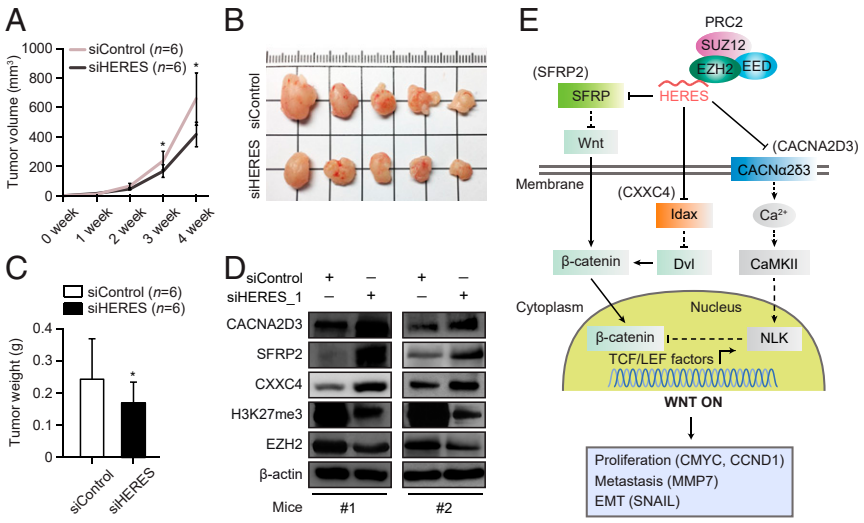

Fig. 7. Expression of HERES regulates tumorigenicity in xenograft models. KYSE-30 cells transfected with either siControl or siHERES were injected into nude mice (6 mice for each group). The resulting xenograft tumor volumes (*A* and *B*) and weights (*C*) are shown. (*A*) Tumor growth curves showing that tumors in the siHERES group grew markedly slower than those in the siControl group. (*B*) Images of tumor volumes from the xenograft models. (*C*) Tumor weights in the siHERES and siControl groups 4 wk after cell injection. Data represent the mean ± SD. (*D*) Immunoblot analysis (#1 and #2) of levels of key components (CACNA2D3, SFRP2, and CXXC4) from the canonical and noncanonical Wnt signaling pathways and of H3K27me3 and EZH2 in the siHERES and siControl xenograft models. (*E*) A graphic illustration of HERES-regulated canonical and noncanonical Wnt signaling pathways in ESCC. $*P \leq 0.05$.

which part of EZH2 interacts with HERES. A previous study showed that the N-terminal region of EZH2 is important for RNA binding through a G-rich motif (41). A series of deletion mutants of human PRC2 revealed that the basic N-terminal helix of EZH2, particularly residues 32–42 in the helix, are the most critical for RNA binding through a G-rich motif. Given these results, the G-rich motif embedded in HERES probably also interacts with the basic N-terminal helix of EZH2, although such a direct interaction needs to be verified.

Transcription factor ChIP-seq data from the ENCODE project revealed that the first *HERES* exon contains some enhancer-related transcription factor binding sites (TFBSs) for CEBPB, EP300, and AP-1 subunits (JUN, FOS) (*SI Appendix*, Fig. S14), suggesting that *HERES* could be regulated epigenetically by modulation of the chromatin state at its locus. On the other hand, the expression of *HERES* near enhancer-related TFBSs raises the possibility that HERES is an enhancer RNA (eRNA) that regulates neighboring genes in *cis*. However, 2 following observations argue against this idea: first, *HERES* is highly abundant and includes both a 5′ cap and 3′ polyadenylation, unlike eRNAs, and second, the genes neighboring *HERES* were only marginally affected by siHERES transfection (*SI Appendix*, Fig. S15).

Although there have been reports that some lncRNAs participate in regulating the Wnt signaling pathway, their targets appear limited (42). Our results suggest that HERES could be a master regulator of the Wnt signaling pathway, because it controls key components of both canonical and Ca^{2+}-related noncanonical pathways (Fig. 7*E*). Our results highlight the potential significance of HERES in terms of targeted therapy, where it could be used to manipulate Wnt signaling pathways and Ca^{2+} homeostasis.

Materials and Methods

Sample Collection and Preparation. Samples from 23 Korean ESCC patients were used for RNA-seq; an additional 43 ESCC patients were also enrolled in this study. Clinicopathological findings and tissues were obtained prospectively (Dataset S6). Cancerous and adjacent noncancerous mucosa tissues were collected by endoscopic biopsy from all 66 ESCC patients, regarded as the YSH (Yonsei Severance Hospital) cohort. Additionally, normal mucosal tissues from 21 patients with reflux symptoms, as well as ESCC cell lines, were used in the study. Immediately after collection, tissues were transferred to RNAlater (Ambion,) and then stored at −80 °C. Total RNA was extracted from ESCC cells and tissues and then subjected to qRT-PCR for construction of RNA-seq libraries (*SI Appendix, Methods* for more details). All tissue samples were obtained after receiving written informed consent from patients according to the Declaration of Helsinki, and this study was approved by Institutional Review Board (IRB) of the Yonsei University College of Medicine (# 4–2011-0891).

Annotations and Expression Profiling of lncRNAs. To profile both annotated and unannotated lncRNAs expressed in ESCC, transcriptome assembly and lncRNA annotations were performed over the initial 13 RNA-seq datasets obtained from the YSH cohort using our computational pipeline (*SI Appendix, Methods* for more details). Using the resulting annotations of all lncRNAs, lncRNA expression levels were measured over the YSH cohort, publicly available ESCC cohorts (95 tumor samples from TCGA and 15 paired samples from a Chinese ESCC cohort) (26, 43), and GTEx Esophagus mucosa datasets (328 samples) (44) (*SI Appendix, Methods* for more details). Because the RNA-seq data from the TCGA ESCC and GTEx Esophagus mucosa datasets were unstranded types (reads with no strand information), the strand information was predicted and the unstranded reads were converted to RPDs (reads with predicted directions) using CAFE (27).

Methylation-Specific PCR (MS-PCR). Genomic DNA was extracted from KYSE-30 cells using a DNeasy Blood and Tissue kit (Qiagen). An EZ DNA Methylation-Gold kit (ZymoResearch) was used for DNA bisulfite transformation. MS-PCR was performed using primers specific for methylated and unmethylated genes (Dataset S9).

ChIP Assay. For chromatin shearing in lysates of cells transfected with small interfering RNA (siRNA) (siHERES or siControl), we used waterbath sonication for 30 cycles under cooling conditions, 15 s on, 30 s off (170–190 W). The fragmented chromatin was extracted using a High-Sensitivity ChIP kit (ab185913; Abcam), according to the manufacturer's protocol. A total of 5 μg of total chromatin was used for ChIP with anti-H3K27me3 (ab6002; Abcam) and the mock immunoprecipitation (IP) (IgG, ab185913; Abcam) at 4 °C overnight. After cross-link reversal and DNA purification, 1 μL of eluted DNA was used for qRT-PCR with target region primers. The primer sequences for qRT-PCR are shown in Dataset S9.

RIP Assay. To immunoprecipitate RNA-protein complexes, cells were first lysed with nuclear isolation buffer (1.28 M sucrose, 40 mM Tris·HCl pH 7.5, 20 mM $MgCl_2$, 4% Triton X-100) and resuspended in RIP buffer (150 mM KCl, 25 mM Tris·HCl pH 7.4, 5 mM EDTA, 0.5 mM DTT, 0.5% Nonidet P-40, 1 U/μL RNase inhibitor, and protease inhibitor). To achieve chromatin shearing, waterbath

sonication was administered for 30 cycles and the lysate was cleared by centrifugation. The appropriate antibody (2 μg) was added to the resulting supernatant (600–800 μg) and the mixture was carefully incubated at 4 °C for 24 h or more on a rotator. After incubation, 20 μL of Magna Chip protein magnetic beads (Merck Millipore) were added, and the solution rotated at 4 °C for 2 h. After washing with RIP buffer, qRT-PCR and Western blotting were carried out following RNA purification with TRIzol reagent or SDS gel electrophoresis, respectively.

Mutagenesis Assay. Mutagenesis of the PRC2-EZH2 binding site in HERES was conducted using a Q5 Site-Directed Mutagenesis kit. HERES_NheI_F acccaagctggctagc GGCAACCAGCTTGCGTCC and HERES_XbaI_r aaacgggccctctaga TTTAAATGA-TAGGGTATTGG were used as the cloning primers to insert the wild-type (WT) HERES cDNA into pcDNA3.1.

HERES-Mut_AS:
TATTTACCTGAATATGTCTTGTATTCATTCATGTAAATTA and

HERES-Mut_S: TAATTTACATGAATGAATA C AAGACATATTCAGGTAAATA primers were used to create HERES-Mut. HERES-Wt and HERES-Mut sequences were confirmed by Sanger sequencing.

Xenograft Assay in Nude Mice. All animal experiments were performed using a protocol approved by Institutional Animal Care and Use Committee at the Catholic University, College of Medicine (2018-0619-01). After transfection of siControl or siHERES, 2×10^6 KYSE-30 cells were suspended in 200 μL of Matrigel solution (BD Biosciences) and s.c. implanted onto the posterior flank of BALB/c nude mice (6-wk-old male, $n = 6$). The volume of the resulting cell mass after 4 wk was measured using a vernier caliper and the mass of each xenograft tumor was analyzed after the animal was euthanized according to the *Guide for the Care and Use of Laboratory Animals* (45).

Data Availability. Raw RNA-seq data and expression tables from ESCC patients have been submitted to the National Center for Biotechnology Information (NCBI) Gene Expression Omnibus (GEO; https://www.ncbi.nlm.nih.gov/geo/) under accession number GSE130078. LncRNA annotation constructed in this study can be downloaded from our website (http://big.hanyang.ac.kr/CASOL/catalog.html).

ACKNOWLEDGMENTS. We thank all Bioinformatics and Genomics (BIG) lab members for critical reading and comments. The results shown here are in part based upon data generated by the TCGA Research Network: https://www.cancer.gov/tcga. The TCGA and GTEx data used in this manuscript were obtained from the database of Genotypes and Phenotypes (dbGaP) through accession numbers phs000178.v10.p8 and phs000424.v6.p1, respectively. This work was supported by Korean Health Technology R&D Project, Ministry of Health and Welfare (HI15C3224) and by the Bio and Medical Technology Development Program and the Basic Science Research Program through the National Research Foundation (NRF), funded by the Ministry of Science and Information and Communication Technologies (ICT) (grant numbers 2017M3A9G8084539, 2017R1A2B4006316, and 2018R1A2B2003782).

1. R. Nusse, H. E. Varmus, Wnt genes. *Cell* **69**, 1073–1087 (1992).
2. P. Polakis, Wnt signaling and cancer. *Genes Dev.* **14**, 1837–1851 (2000).
3. F. Deng, K. Zhou, W. Cui, D. Liu, Y. Ma, Clinicopathological significance of wnt/β-catenin signaling pathway in esophageal squamous cell carcinoma. *Int. J. Clin. Exp. Pathol.* **8**, 3045–3053 (2015).
4. T. Zhan, N. Rindtorff, M. Boutros, Wnt signaling in cancer. *Oncogene* **36**, 1461–1473 (2017).
5. T. Grigoryan, P. Wend, A. Klaus, W. Birchmeier, Deciphering the function of canonical Wnt signals in development and disease: Conditional loss- and gain-of-function mutations of beta-catenin in mice. *Genes Dev.* **22**, 2308–2341 (2008).
6. H. Clevers, Wnt/beta-catenin signaling in development and disease. *Cell* **127**, 469–480 (2006).
7. M. V. Semenov, R. Habas, B. T. Macdonald, X. He, SnapShot: Noncanonical Wnt signaling pathways. *Cell* **131**, 1378 (2007).
8. R. T. Moon, A. D. Kohn, G. V. De Ferrari, A. Kaykas, WNT and beta-catenin signalling: Diseases and therapies. *Nat. Rev. Genet.* **5**, 691–701 (2004).
9. J. N. Anastas, R. T. Moon, WNT signalling pathways as therapeutic targets in cancer. *Nat. Rev. Cancer* **13**, 11–26 (2013).
10. V. Conteduca *et al.*, Barrett's esophagus and esophageal cancer: An overview. *Int. J. Oncol.* **41**, 414–424 (2012).
11. K. J. Napier, M. Scheerer, S. Misra, Esophageal cancer: A review of epidemiology, pathogenesis, staging workup and treatment modalities. *World J. Gastrointest. Oncol.* **6**, 112–120 (2014).
12. S. Ohashi *et al.*, Recent advances from basic and clinical studies of esophageal squamous cell carcinoma. *Gastroenterology* **149**, 1700–1715 (2015).
13. K. Higuchi *et al.*, Current management of esophageal squamous-cell carcinoma in Japan and other countries. *Gastrointest. Cancer Res.* **3**, 153–161 (2009).
14. Y. Miyawaki *et al.*, Efficacy of docetaxel, cisplatin, and 5-fluorouracil chemotherapy for superficial esophageal squamous cell carcinoma. *Dis. Esophagus* **30**, 1–8 (2017).
15. M. W. Wiedmann, J. Mössner, New and emerging combination therapies for esophageal cancer. *Cancer Manag. Res.* **5**, 133–146 (2013).
16. X. Kang *et al.*, Personalized targeted therapy for esophageal squamous cell carcinoma. *World J. Gastroenterol.* **21**, 7648–7658 (2015).
17. C. P. Ponting, P. L. Oliver, W. Reik, Evolution and functions of long noncoding RNAs. *Cell* **136**, 629–641 (2009).
18. I. Ulitsky, D. P. Bartel, lincRNAs: Genomics, evolution, and mechanisms. *Cell* **154**, 26–46 (2013).
19. M. Huarte, The emerging role of lncRNAs in cancer. *Nat. Med.* **21**, 1253–1261 (2015).
20. J. F. Collins, Long noncoding RNAs and hepatocellular carcinoma. *Gastroenterology* **148**, 291–294 (2015).
21. A. M. Schmitt, H. Y. Chang, Long noncoding RNAs in cancer pathways. *Cancer Cell* **29**, 452–463 (2016).
22. J. H. Yuan *et al.*, A long noncoding RNA activated by TGF-β promotes the invasion-metastasis cascade in hepatocellular carcinoma. *Cancer Cell* **25**, 666–681 (2014).
23. M. M. Ali *et al.*, PAN-cancer analysis of S-phase enriched lncRNAs identifies oncogenic drivers and biomarkers. *Nat. Commun.* **9**, 883 (2018).
24. Y. Wu *et al.*, Up-regulation of lncRNA CASC9 promotes esophageal squamous cell carcinoma growth by negatively regulating PDCD4 expression through EZH2. *Mol. Cancer* **16**, 150 (2017).
25. J. H. Yoon *et al.*, The long noncoding RNA LUCAT1 promotes tumorigenesis by controlling ubiquitination and stability of DNA methyltransferase 1 in esophageal squamous cell carcinoma. *Cancer Lett.* **417**, 47–57 (2018).
26. C. Q. Li *et al.*, Integrative analyses of transcriptome sequencing identify novel functional lncRNAs in esophageal squamous cell carcinoma. *Oncogenesis* **6**, e297 (2017).
27. B. H. You, S. H. Yoon, J. W. Nam, High-confidence coding and noncoding transcriptome maps. *Genome Res.* **27**, 1050–1062 (2017).
28. A. R. Forrest *et al.*; FANTOM Consortium and the RIKEN PMI and CLST (DGT), A promoter-level mammalian expression atlas. *Nature* **507**, 462–470 (2014).
29. J. W. Nam *et al.*, Global analyses of the effect of different cellular contexts on microRNA targeting. *Mol. Cell* **53**, 1031–1043 (2014).
30. Y. Li *et al.*, Investigation of tumor suppressing function of CACNA2D3 in esophageal squamous cell carcinoma. *PLoS One* **8**, e60027 (2013).
31. A. Wanajo *et al.*, Methylation of the calcium channel-related gene, CACNA2D3, is frequent and a poor prognostic factor in gastric cancer. *Gastroenterology* **135**, 580–590 (2008).
32. A. M. Wong *et al.*, Characterization of CACNA2D3 as a putative tumor suppressor gene in the development and progression of nasopharyngeal carcinoma. *Int. J. Cancer* **133**, 2284–2295 (2013).
33. H. Zou *et al.*, Aberrant methylation of secreted frizzled-related protein genes in esophageal adenocarcinoma and Barrett's esophagus. *Int. J. Cancer* **116**, 584–591 (2005).
34. M. T. Chung *et al.*, SFRP1 and SFRP2 suppress the transformation and invasion abilities of cervical cancer cells through Wnt signal pathway. *Gynecol. Oncol.* **112**, 646–653 (2009).
35. E. Viré *et al.*, The Polycomb group protein EZH2 directly controls DNA methylation. *Nature* **439**, 871–874 (2006).
36. H. Cedar, Y. Bergman, Linking DNA methylation and histone modification: Patterns and paradigms. *Nat. Rev. Genet.* **10**, 295–304 (2009).
37. T. Kojima *et al.*, Decreased expression of CXXC4 promotes a malignant phenotype in renal cell carcinoma by activating Wnt signaling. *Oncogene* **28**, 297–305 (2009).
38. M. Guttman, J. L. Rinn, Modular regulatory principles of large non-coding RNAs. *Nature* **482**, 339–346 (2012).
39. X. Wang *et al.*, Targeting of polycomb repressive complex 2 to RNA by short repeats of consecutive guanines. *Mol. Cell* **65**, 1056–1067.e5 (2017).
40. Y. Lubelsky, I. Ulitsky, Sequences enriched in Alu repeats drive nuclear localization of long RNAs in human cells. *Nature* **555**, 107–111 (2018).
41. Y. Long *et al.*, Conserved RNA-binding specificity of polycomb repressive complex 2 is achieved by dispersed amino acid patches in EZH2. *eLife* **6**, e31558 (2017).
42. V. Zarkou, A. Galaras, A. Giakountis, P. Hatzis, Crosstalk mechanisms between the WNT signaling pathway and long non-coding RNAs. *Noncoding RNA Res.* **3**, 42–53 (2018).
43. Cancer Genome Atlas Research Network *et al.*, Integrated genomic characterization of oesophageal carcinoma. *Nature* **541**, 169–175 (2017).
44. GTEx Consortium, The Genotype-tissue expression (GTEx) project. *Nat. Genet.* **45**, 580–585 (2013).
45. National Research Council, *Guide for the Care and Use of Laboratory Animals* (National Academies Press, Washington, DC, ed. 8, 2011).